Effects of Finite Height Topography on Nongeostrophic Baroclinic Instability: Implications to Theories of Lee Cyclogenesis

P. MALGUZZI, A. TREVISAN AND A. SPERANZA

CNR Fisbat, Bologna, Italy

(Manuscript received 3 February 1986, in final form 4 November 1986)

ABSTRACT

Baroclinic instability in the presence of steep finite amplitude topography is studied in the primitive equation model. The quasi-geostrophic theory of Alpine cyclogenesis of Speranza et al. is reanalyzed and discussed in this context.

The present model is a generalization of the one used by Stone to include topographic effects, lateral shear of the basic wind, and/or lateral walls. We focus in particular on the differences between this formulation and the quasi-geostrophic one when the meridional scale of the topography is very small (of the order of 100 km). We find that only in the primitive equation model does a small-volume mountain, of height and width comparable with those of the Alps, introduce significant large-scale modifications to the baroclinic modes. The most unstable mode attains its maximum amplitude to the southern side of the mountain. We show that these results do not depend upon the specification of the lateral boundary conditions provided the basic state baroclinicity is meridionally confined.

1. Introduction

In previous studies (Speranza et al., 1985; Buzzi and Speranza, 1986, hereafter referred to as Part I and Part II, respectively), the problem of how baroclinically unstable normal modes are modified by localized topography was analyzed in the context of the quasi-geostrophic model. While the modifications of the spatial structure of baroclinically unstable modes were able to account for the observed structure of Alpine lee cyclogenesis, doubts were raised as to the validity of the results obtained with the quasi-geostrophic approximation when dealing with high and steep mountains. The same problem is analyzed herein using primitive equations.

Quasi-geostrophic models are able to reproduce the observed characteristics of Alpine cyclogenesis, when slope effects are taken into account (Smith, 1984; Trevisan et al., 1984; Part I and Part II). In all these cases, however, it is necessary to introduce extremely large-volume mountains in order to produce significant lee disturbances. It will be shown that the quasi-geostrophic model gives completely erroneous results, when dealing with narrow mountains: a barrier-type effect is observed, which causes the normal modes to be symmetrically split by the ridge in a fashion similar to the one studied by Pierrehumbert (1985), observed in the limit of a vertical wall. The primitive equation model presented here is not affected by such hindrances; the spatial modifications of the baroclinic modes, due to the presence of a high, narrow ridge, present the desired symmetry properties for the physical example we have in mind. For obvious practical reasons, only the infinite ridge is considered in the present study; an extension to the case of an isolated mountain would be desirable. However, we think that the extension of the quasi-geostrophic results to the three-dimensional case (Part I and Part II) is suggestive of what can be expected in the primitive case also.

Besides lee cyclogenesis, the other strong motivation for the present study is to show that narrow regions of ageostrophy can strongly influence the large scale quasi-geostrophic motion. In this work, we consider a standard atmosphere having a bulk Richardson number consistent with quasi-geostrophic dynamics on synoptic scales and forced by boundary dishomogeneities on a small scale (of the order of 100 km) which locally introduce a large Rossby number. Stone (1966) analyzed the problem of nongeostrophic baroclinic instability in the Eady model without orography. He showed that the quasi-geostrophic eigenmodes and eigenvalues were not significantly modified by nongeostrophic dynamics for large Richardson number regimes. It is conceivable that the slow baroclinic modes in which we are interested will be in quasi-geostrophic balance far away from the region of small scale forcing. What is not obvious a priori is the fact that even their large-scale structure is strongly modified (with respect to the solution of the quasi-geostrophic system) by the presence of such forcing, as will be shown later. In fact, the solution consists of "patches" of regions of quasi-geostrophic motion, matched together by a narrow region of ageostrophic

motion. For this reason, the quasi-geostrophic system cannot furnish the exact solution over the whole domain.

In section 2 the scaled model equations and boundary conditions are set up and a brief description is given of the numerical method used to find the eigenvalues and eigenvectors. In section 3, results are shown for a set of parameters typical of a standard baroclinic atmosphere for a ridge of height and width comparable to those of the Alps: the effects of lateral boundary conditions and lateral shear in the basic state current are investigated. The robustness of the solution is checked against variations of the physical and geometrical parameters and model resolution. Comparisons with the results obtained using the quasi-geostrophic model are discussed in section 4. In section 5 we draw our conclusions.

2. The model

Let us consider the equations of motion in the hydrostatic and quasi-Boussinesq approximation:

$$\left.\begin{aligned} &u_t+uu_x+vu_y+wu_z-f_0v=-\phi_x\\ &v_t+uv_x+vv_y+wv_z+f_0u=-\phi_y\\ &g\theta/\theta_s=\phi_z\\ &\theta_t+u\theta_x+v\theta_y+w\theta_{sz}=0\\ &u_x+v_y+w_z=0 \end{aligned}\right\} \quad (2.1)$$

where the following definitions have been made:

- f_0 Coriolis parameter, assumed constant,
- ϕ P/ρ_s, $\rho_s(z)$ density corresponding to the background stratification and p pressure,
- Θ $\theta_s(z)+\theta(x, y, z, t)$ where Θ is the potential temperature and θ_s represents the background stratification,
- g gravity.

Let us introduce the basic state:

$$\bar{u}(y, z)=m^*(y)z \quad (2.2)$$

which is a generalization of the basic profile of the Eady problem. Thus

$$\left.\begin{aligned} &u=\bar{u}+u'\\ &v=v'\\ &w=w'\\ &\theta=-\theta_s\frac{f_0}{g}\int\bar{u}_z dy+\frac{\theta_s}{g}\theta'\\ &\phi_z=-f_0\int\bar{u}_z dy+\phi'_z \end{aligned}\right\} \quad (2.3)$$

Substituting (2.3) into (2.1) and linearizing around (2.2) it follows that

$$\left.\begin{aligned} &u'_t+\bar{u}u'_x+v'\bar{u}_y+w'm^*-f_0v'=-\phi'_x\\ &v'_t+\bar{u}v'_x+f_0u'=-\phi'_y\\ &\phi'_z=\theta'\\ &\theta'_t+\bar{u}\theta'_x-v'f_0m^*+N^2w'=0\\ &u'_x+v'_y+w'_z=0 \end{aligned}\right\} \quad (2.4)$$

where $N^2=g\theta_{sz}/\theta_s$ is the Brunt–Väisälä frequency assumed to be constant.

Let us render the equations dimensionless by introducing the following scales (Stone, 1966):

- U horizontal velocity scale,
- H vertical scale equal to the depth of the atmosphere,
- U/f_0 x and y scales,
- Hf_0 vertical velocity scale,
- f_0^{-1} time scale.

In these units, the only dimensionless numbers (besides the mountain parameters) entering the problem are the Richardson number $\mathrm{Ri}=N^2H^2/U^2$, which is a large number if "bulk" values for U and N^2 are taken, and the dimensionless vertical shear $m=m^*H/U$.

The solution of (2.4) is written in the normal mode form as

$$\phi'=\hat{\phi}(y, z)e^{ik(x-ct)}$$

and similarly for u', v', w'. A unique equation for $\hat{\phi}$ can be obtained by substituting the expressions of $\hat{u}$, $\hat{v}$, $\hat{w}$ in terms of $\hat{\phi}$ in the continuity equation; these are expressions derived from the momentum and thermodynamic equations.

The lower (upper) boundary condition is $\hat{w}=\hat{v}h_y$ computed at $z=h(y)$ ($\hat{w}=0$ at $z=1$). As lateral boundary conditions, we shall impose either periodicity or $\hat{v}=0$ (lateral walls) at $y=-L_y/2$, $L_y/2$.

In order to transform the y–z domain into a rectangular one, the vertical coordinate

$$\eta=\frac{z-h}{1-h}$$

is introduced.

The meridional structure of the geopotential is governed by the following equation and boundary conditions

$$\hat{\phi}_{\eta\eta}+C_1\hat{\phi}_{yy}+C_2\hat{\phi}_{y\eta}+C_3\hat{\phi}_y+C_4\hat{\phi}_\eta+C_5\hat{\phi}=0 \quad (2.5a)$$

$$\hat{\phi}_\eta+\alpha_{0,1}\hat{\phi}_y+\beta_{0,1}\hat{\phi}=0, \quad \eta=0, 1$$

$$\hat{\phi}_y+\frac{m}{\mathrm{Ri}}\hat{\phi}_\eta-\frac{1}{mz-c}\hat{\phi}=0 \quad (\hat{v}=0) \quad (2.5b)$$

or periodicity

$$y=-L_y/2, L_y/2$$

where the coefficients C_n, $\alpha_{0,1}$, $\beta_{0,1}$ are lengthy expressions involving y, η, k, Ri, $m(y)$, $h(y)$ and the eigenvalue c.[1]

[1] See Appendix.

Equations (2.5) were solved numerically by defining $\hat{\phi}$ and the coefficients over a bidimensional grid on the y, η domain. The problem is thus reduced to that of finding the values of c which cancel the determinant of the matrix obtained from the discretization of (2.5). We briefly describe the algorithm used to find the eigenvalues. Let c^* be the (complex) eigenvalue of the problem, i.e., if D denotes the determinant, $D(c^*) = 0$. Let c^{I}, c^{II} be two initial guesses of the eigenvalue; then

$$D(c^{\mathrm{I}}) = D(c^*) + \frac{d}{dc}D(c^*)(c^{\mathrm{I}} - c^*) + \cdots \quad (2.6)$$

$$D(c^{\mathrm{II}}) = D(c^*) + \frac{d}{dc}D(c^*)(c^{\mathrm{II}} - c^*) + \cdots. \quad (2.7)$$

Eliminating dD/dc between (2.6) and (2.7) we get an expression for c^* which can be used as the next guess. In general, (2.6) and (2.7) suggest the following iteration procedure:

$$c^{n+1} = \frac{c^{n-1}D(c^n) - c^nD(c^{n-1})}{D(c^n) - D(c^{n-1})}.$$

This procedure gives a very accurate estimate of c^* (<0.1%) with just a few iterations. Starting with $h_0 = 0$ an adequate first guess is given by the eigenvalues of the Eady problem without a mountain. For a given shape of the topography, the height of the mountain is then gradually increased from zero to the desired value, using as a guess the eigenvalue corresponding to the value of h_0 used in the previous step. Convergence at each step is reached before moving on to a higher topography.

3. Results

The linear model which produced the encouraging results in Part I was not completely satisfactory, because of the many simplifying assumptions introduced. In the present case, primitive equations are used instead of the quasi-geostrophic set and a realistically high and steep mountain is considered. Furthermore, the effects of applying the lower boundary condition at $z = h$ instead of $z = 0$ are investigated together with those produced by the lateral boundary conditions and by the introduction of a meridionally dependent, baroclinic basic state current.

It is important to discover how the structure of the normal modes found in Part I is modified by these model improvements and, above all, whether the asymmetries observed in lee cyclogenesis survive the complexities of the present model. In particular, the role of the ageostrophic part of the motion, expected to be particularly intense when steep mountains are present, will be investigated. We start by showing one example considered typical for the physical application we have in mind. Subsequently, by varying the parameters (within acceptable limits), we shall test the robustness of our findings.

We chose the following parameters as typical of the basic zonal wind, stratification and geometry:

$f_0 = 10^{-4}$

Vertical scale $H = 10$ km

$U = 30\ \mathrm{m\ s^{-1}}$ (horizontal scale = $U/f_0 = 300$ km)

Ri = 10 ($N^2 = 0.9\ 10^{-4}\ \mathrm{s^{-2}}$)

Mountain width (at the base) $y_0 = 1$ (300 km)

Mountain height $h_0 = 0.2$ (2 km)

Domain width $L_y = 16.666$ (5000 km). (3.1)

The value of U represents the mean zonal wind at $z = H$ (tropopause). Thus, when no meridional shear is present, $\bar{u} = z$ ($m = 1$) in dimensionless units. The zonal wavenumber of the growing perturbation is $k = 0.4$ (wavelength $\sim$ 4700 km) which is between that of the most unstable wave and one appropriate for Alpine cyclogenesis. The height and width of the mountain have been chosen bearing in mind a steep mountain chain like the Alps. The simplest shape, a triangular mountain, has been chosen for the pictures produced here, since the results obtained with different topographies did not depend on the details of the profile.

Figure 1 shows the two unstable eigenmodes obtained with the above parameters and with $m = 1$ (no horizontal shear) and lateral walls at $y = -L_y/2$, $L_y/2$. The resolution employed here is 61 grid points in the meridional domain ($dy \sim 80$ km) by 15 vertical levels. The structure of the most unstable mode is characteristic of a developing baroclinic wave confined in the southern half of the domain, while the second most unstable normal mode (Fig. 1b) reaches its maximum amplitude in the northern half of the channel. The most unstable eigenmode depicted in figure 1a originates from the gravest mode without orography (see Fig. 2), which is symmetric around the center of the channel. As the height of the mountain increases, the mode reaches the strong degree of asymmetry which makes it important for Alpine cyclogenesis. It should be noted that this mode is the most unstable one also in the physically more interesting case of a sheared basic current. Figure 2 shows the imaginary part of the phase speed of all unstable modes versus the mountain height for the values of the parameters listed above. One set of curves corresponds to the case $m = 1$, and the other to a velocity profile given by $m = 1 + 0.25 \times \cos(2\pi y/L_y)$, both profiles having the same mean baroclinicity. The most unstable eigenmode is not significantly modified by the introduction of meridional shear (and consequently it is not shown), while the second and third exchange their identities. The third unstable normal mode (Fig. 3) is strongly confined to the northern slope of the mountain and quickly disappears, as the mountain height is increased beyond $\sim$1 km.

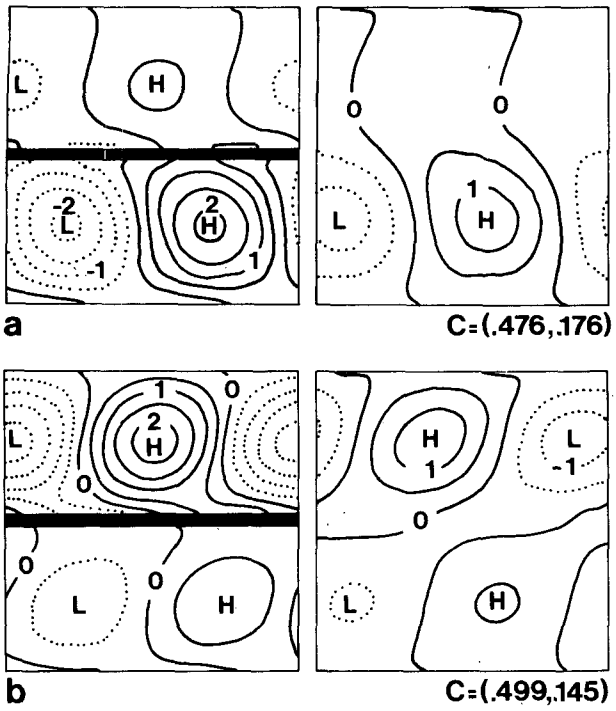

FIG. 1. (a) Geopotential ϕ at $z = 0.1$ and $z = 0.5$ for the most unstable eigenmode in the channel. Ridge height $h_0 = 0.2$, (2 km), width $y_0 = 1$ (300 km). Basic state current without horizontal shear ($m = 1$). The parameter values are Ri = 10, $k = 0.4$, $L_y = 16.6$ (5000 km). The intersection with the ridge has been shaded black. All the geopotential patterns shown in the following are normalized in such a way that $\int_0^1 \int_{-L_y/2}^{L_y/2} |\phi|^2 dy d\eta = 1$. Contour interval, unless otherwise stated, is 0.5. (b) As in (a) but for the second most unstable eigenmode. The value of c is indicated below each eigenmode.

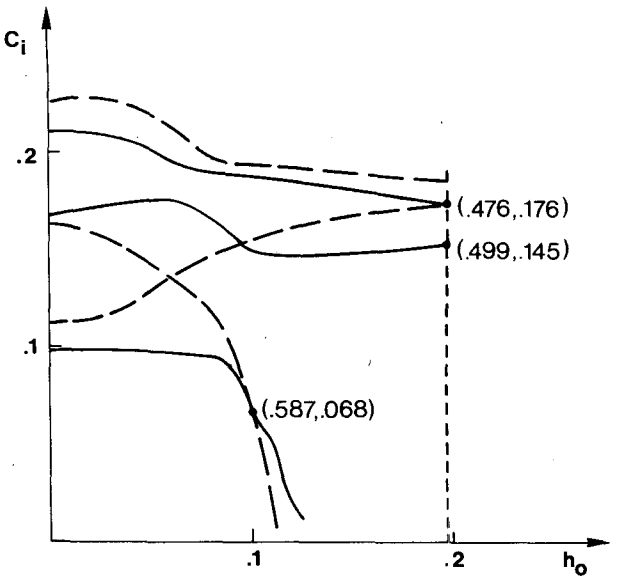

FIG. 2. Imaginary part of the phase speed c as a function of ridge height h_0 for the first three most unstable modes and for basic state current without meridional shear ($m = 1$; continuous line) and with meridional shear ($m = 1 + 0.25 \cos(2\pi y/L_y)$; dashed line). Other parameters as in Fig. 1. The growth rates of the normal modes shown in Figs. 1 and 3 are in parentheses.

With regard to the symmetry properties of these modes, in order to fully understand the implications of choosing the physically most appropriate basic state, we should make a brief digression. The reason why the same type of modes may exist in the channel with or without lateral shear is that the presence of walls has a confining effect. If periodic lateral boundary conditions are used, the most unstable mode naturally extends across the periodic boundary (see Fig. 4a). However, if a basic state with meridional shear is introduced in the periodic domain, the same type of asymmetric mode found in the presence of lateral walls is recovered (Fig. 4b), since the normal mode is confined within the latitudinal belt possessing baroclinicity (Stone, 1969; Simmons, 1974).

The nongeostrophic meridional velocity, superposed on the pressure pattern, is shown in Fig. 5a. The nongeostrophic part of the motion opposes the geostrophic flow everywhere on the mountain, thus reducing the vertical velocity due to slope effects. Nevertheless, the vertical velocity is still well correlated with the geostrophic flow, as clearly indicated by Fig. 5b. The pattern of nongeostrophic meridional velocity deflects part of the low level flow along the mountain chain, thus indicating a mountain-induced blocking effect. The relative strength of the geostrophic motion to the ageostrophic one over the mountain can be estimated to be in the ratio of 2:1 in the case shown in Fig. 5. To establish the connection between this linear theory and the results relative to blocking effects due to mesoscale mountains (Pierrehumbert, 1984, Pierrehumbert and Wyman, 1985), we estimate the parameters Ro and RoFr where Ro and Fr indicate, respectively, the Rossby number and the Froude number

$$\mathrm{Ro} = \frac{v'}{f_0 y_m}, \quad \mathrm{Fr} = \frac{N h_m}{v'}$$

where h_m and y_m are the dimensional mountain height and width, respectively based on the "upstream" ve-

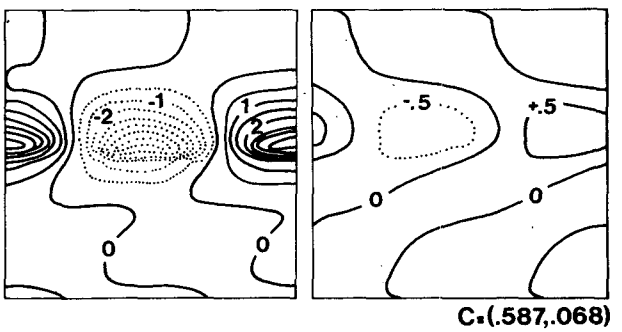

FIG. 3. Geopotential ϕ for the third most unstable eigenmode at $z = 0.1$ and $z = 0.5$. Other parameters as in Fig. 1, except for $h_0 = 0.1$.

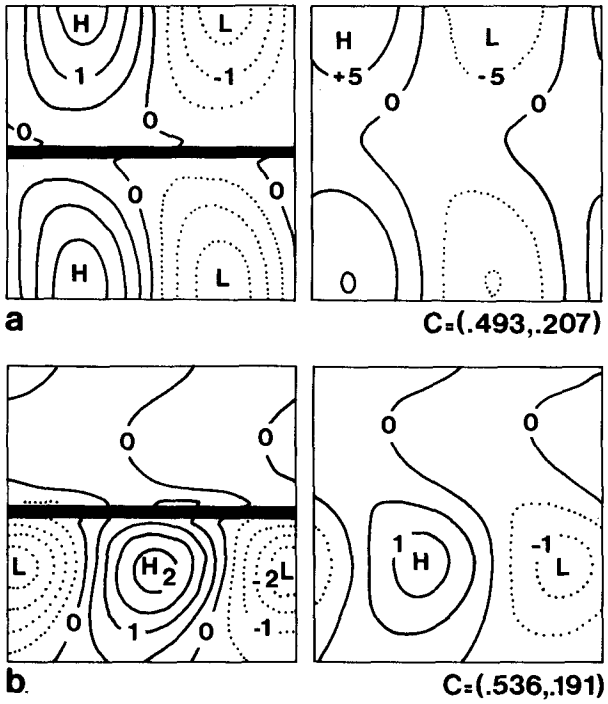

FIG. 4. Geopotential ϕ for the most unstable eigenmode at $z = 0.1$ and $z = 0.5$ in a domain with periodic lateral boundary conditions (a) without meridional shear ($m = 1$), and (b) with meridional shear ($m = 1 + 0.25 \cos(2\pi y/L_y)$). Other parameters as in Fig. 1.

locity v' impinging over the ridge. Since this theory is linear, Ro is arbitrarily small so that the wind over the topography will deviate greatly from the geostrophic balance whenever RoFr > O(1), but will remain nearly geostrophic when RoFr $\ll$ 1 (Pierrehumbert and Wyman, 1985). In our notations, RoFr is equal to $\sqrt{\text{Ri}}h_0/y_0$, which is independent of the perturbation velocity v'. The case of Fig. 5 is characterized by $\sqrt{\text{Ri}}h_0/y_0 = 1.26$ so that the blocking effect of the mountain is consistently strong. Figure 6 depicts a different case characterized by $\sqrt{\text{Ri}}h_0/y_0 = 0.12$. The ageostrophic velocity (not shown) is an order of magnitude smaller than the geostrophic flow over the mountain, indicating the absence of blocking effects. We stress that in the present theory the occurrence of lee cyclogenesis is independent of any blocking of the low-level flow, as clearly indicated by Figs. 1a and 6.

In order for these findings to be significant, they should be proven to be independent of the particular setting of the parameters we have chosen. To this end, the height and width of the mountain have been varied, as well as the external parameters (k, Ri, L_y). If these variations are restricted to physically acceptable ranges, (wavelength between 3000 and 6000 km, mountain height 1 to 3 km, mountain width 200 to 500 km, 2 < Ri < 100) the behavior of our solutions is not essentially modified. In particular, the structure of the most unstable mode is insensitive to the horizontal resolution employed, while the asymmetry of the eigenmode is found to increase slightly with increasing vertical resolution.

4. The limits of the quasi-geostrophic approximation

The two most unstable eigenmodes obtained using the quasigeostrophic model with $m = 1$ (Eady model) are shown in Figs. 7a, b. These modes are computed by means of the numerical procedure described in section 2, where all nongeostrophic terms are dropped. In par-

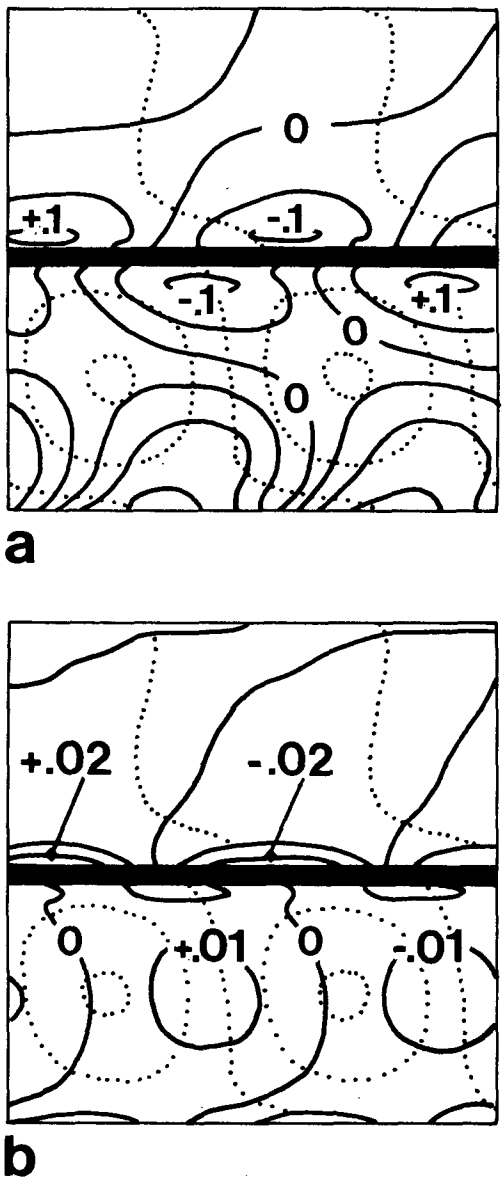

FIG. 5. (a) Meridional component of ageostrophic velocity at $z = 0.1$ (continuous line; contour interval = 0.05) and (b) vertical velocity at $z = 0.1$ (continuous line; contour interval = 0.01) superposed on the geopotential (dashed; contour interval = 1) of the most unstable eigenmode of Fig. 1.

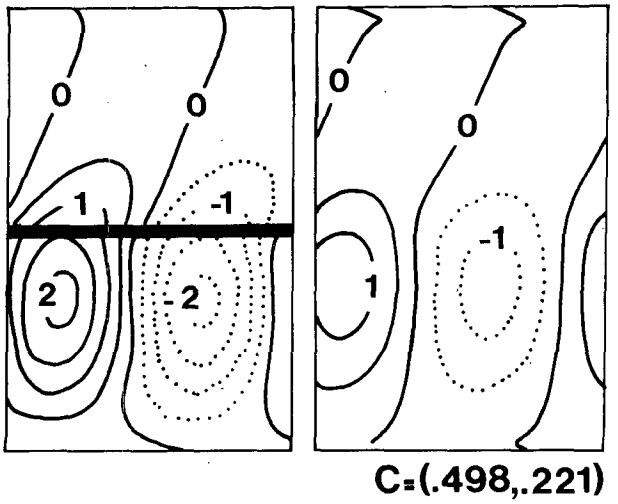

FIG. 6. Geopotential ϕ for the most unstable eigenmode at $z = 0.09$ and $z = 0.5$ for the following setting of the basic state parameters and ridge geometry: Ri = 4, $k = 0.6$, $m = 1$, $h_0 = 0.1$, $y_0 = 3.2$ ($\sim$1000 km).

ticular, the lower boundary condition is applied at $z = 0$ and the lateral boundary conditions assume the geostrophic form $\hat{\phi} = 0$ at $y = -L_y/2, L_y/2$. The parameters are as in (3.1). The differences between the quasi-geostrophic and the primitive dynamics (Figs. 1a, b) are remarkable in the case under examination. The steep mountain "cuts" the most unstable eigenmode (which would naturally extend across the center of the channel) into two pieces of almost equal amplitude; the asymmetries characteristic of the most unstable normal mode are thus lost in the quasi-geostrophic dynamics. The second most unstable normal mode has its nodal line over the ridge and is not affected by the orography. Similar characteristics are found by Pierrehumbert (1985) and Speranza et al. (1985), who studied similar instability problems in two layer models with a vertical wall blocking the meridional flow at the lower level. In other words, in the quasi-geostrophic model a steep ridge acts like a barrier blocking the low level flow.

The differences between the two formulations of the baroclinic instability problem in the presence of steep orography are undoubtedly striking, especially since such differences are not confined to the regions near the mountain (where nongeostrophy is important), but extend throughout the whole domain. This result casts some doubts on those theoretical problems analyzed in the context of quasi-geostrophic dynamics in which interaction with orography plays a crucial role.

A deeper understanding of the mathematical nature of the problem can be inferred by considering the nongeostrophic terms as a perturbation of the quasi-geostrophic dynamics. Formally, the simplest way of doing this consists in multiplying the nongeostrophic terms in (A1)–(A4) by a perturbative parameter ϵ. Of course, the physical case corresponds to $\epsilon = 1$ but we allow ϵ to vary in the complex plane, in order to look for singularities of the dispersion relation $c = c(\epsilon)$ (see Bender-Orzag, 1978); these singularities determine the radius of convergence of a hypothetical power series of ϵ. If the radius of convergence is very small, nongeostrophic effects can by no means be considered as a simple perturbation of the quasi-geostrophic problem. Thus, large differences can be expected between the "perturbed" and "unperturbed" dynamics. On the other hand, radii of convergence much larger than 1 imply negligible nongeostrophic effects. Note that the eigenvalue reflects large-scale differences between the spatial structure of the quasi-geostrophic and primitive eigenmodes. In fact, the eigenvalue is a global property of the eigenmode and, as such, it is not sensitive to differences with limited regional extension compared to the whole domain.

The search for the singularities of $c = c(\epsilon)$, as a function of the parameters characterizing the topography, is not an easy task, given the involved nature of the problem (see Appendix). Since the dispersion relation is multivalued, the kind of singularity we should expect is a branch point. A simple way to determine whether a branch point falls inside or outside the circle of radius 1 in the complex ϵ-plane is to follow the considered branch of $c(\epsilon)$ along the unitary circle $\epsilon = \exp(i\theta)$, $\theta \in (0, 2\pi)$. If, after one lap, a different branch is found, then a branch point exists for $|\epsilon| < 1$ (level crossing).

This technique was applied to mountains of different

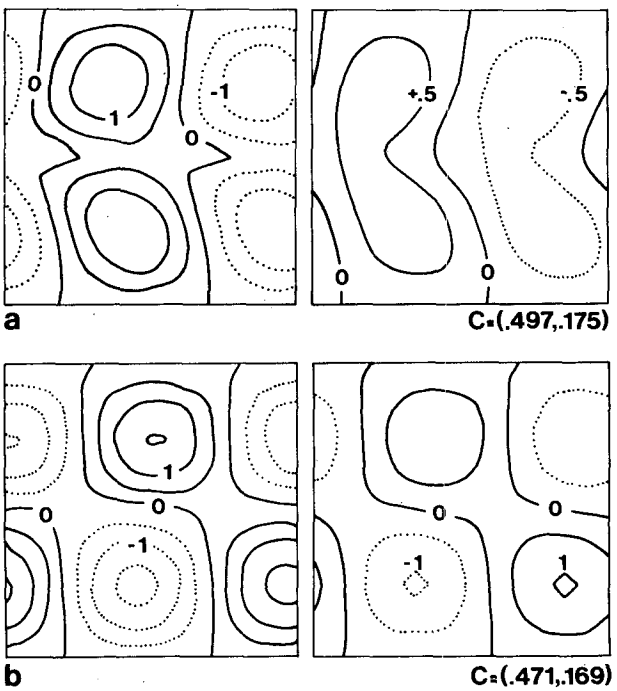

FIG. 7. Geopotential ϕ for (a) the first and (b) the second most unstable eigenmodes of the quasi-geostrophic model. The geometry and the parameter values are as in Fig. 1.

heights and widths. Level crossing of the most unstable eigenvalue with another branch of the dispersion relation (usually the second or third most unstable eigenvalue) occurred close to the origin, when high and steep mountains were dealt with. For mountains consistent with the quasi-geostrophic approximation, level crossing did not occur inside the unitary circle.

We have shown that the breakdown of the quasi-geostrophic dynamics can be brought back to the existence of a singularity of $c(\epsilon)$ near the origin. This procedure, which gives results in agreement with the qualitative behavior mentioned previously, can be used in general to determine rigorously the validity of a certain approximation perturbed by external or dynamical effects.

5. Conclusions

The hypothesis that Alpine cyclogenesis can be explained in terms of topographically modified baroclinic normal modes may be reconciled with most observational and experimental evidence. The main criticism of its first, quasi-geostrophic formulation (Part I) has been overcome in the present extension to primitive equations. In this case, mountains as narrow and steep as the Alps are sufficient to cause the far-field modifications of the undisturbed baroclinic modes, explaining the dipole difference fields of mountain–no mountain experiments.

One major advantage of our theory is that it accounts for the energy source of the disturbance. This is by no means a secondary aspect, if our aim is to explain the cases of cyclogenesis giving rise to a deep trough or cutoff low at 500 mb. The importance of this aspect is further clarified in the discussion that follows.

Lee cyclogenesis usually takes place when a cold front, associated with a developing baroclinic wave, interacts with the Alps. Radinovich (1965), and more recently Mesinger and Pierrehumbert (1985), put forward the hypothesis that lee pressure deepening may be the consequence of a readjustment to low-level blocking of cold air. It has been observed that the frontal passage and its deformation are associated to the initiation of a shallow lee depression; they do not account, however, for the upper-level deepening of the cyclone, which is characterized by substantial baroclinic energy conversions (Tibaldi et al., 1980). This behavior is confirmed by a numerical experiment, (Tosi et al., 1983) in which the deformation of the thermal field by the mountain (computed as the difference between mountain and no-mountain experiments after the frontal passage) was imposed to simulate this effect in a flat bottom case. The pressure low was quite substantial but shallow, and never developed into a really deep cyclone. This was also the case of another experiment, in which the mountain was removed after the initial cyclone growth.

The importance of the presence of the mountain can be easily interpreted in terms of the normal mode theory. For the assessment of the role of the differential blocking, we advance two hypothesis. On one hand, differential blocking could be the starting mechanism which allows, in a short time span, the creation of a finite amplitude disturbance projecting on to the normal mode. With a mountain of limited east–west extension, a similar mechanism may be necessary to reduce the time of set up of the normal mode. A failure of a prediction model to reproduce the frontal blocking and the initial shallow depression (due to insufficient resolution or other deficiencies in representing the mountain) would also cause a failure to initiate the baroclinic process leading to lee cyclogenesis. On the other hand, frontal deformation may very well be a distinctive feature of the normal mode itself. The evidence that its time evolution is very complicated in the presence of three-dimensional topography is given, for instance, in Pierrehumbert (1985). In fact, despite the simplicity of Pierrehumbert's model, flow splitting and discontinuous turning of the low-level wind around the tip of his semiinfinite wall were found to develop from the incoming northwesterly jet. Clearly, a deeper understanding of this matter could come from the analysis of baroclinic instability in the presence of three-dimensional topography.

APPENDIX

Equation Coefficients

In the following we give the expressions for the coefficients appearing in Eq. (2.5). The equation for $\hat{\phi}(y, z)$ in Cartesian coordinates is

$$b_{11}\hat{\phi}_{yy} + b_{22}\hat{\phi}_{zz} + b_{12}\hat{\phi}_{yz} + b_1\hat{\phi}_y + b_2\hat{\phi}_z + b\hat{\phi} = 0 \quad \text{(A1)}$$

where, by denoting with $u_D = mz - c$ the Doppler-shifted velocity,*

$$\left.\begin{aligned}
b_{11} &= \underline{-u_D\,\mathrm{Ri}} \\
b_{22} &= u_D(\kappa^2 u_D{}^2 \underline{-1} + u_{Dy}) \\
b_{12} &= -2u_D m \\
b_1 &= \frac{D_y}{D}u_D\,\mathrm{Ri} + \frac{D_z}{D}u_D m \\
b_2 &= 2m\kappa^2 u_D{}^2 + \frac{D_y}{D}u_D m - \frac{D_z}{D}u_D(\kappa^2 u_D{}^2 - 1 + u_{Dy}) \\
b &= \underline{\kappa^2 u_D\,\mathrm{Ri}} + 2\kappa^2\,\mathrm{Ri}u_D u_{Dy} + 2mu_{Dy} + \mathrm{Ri}u_{Dyy} \\
&\quad - \frac{D_y}{D}(\kappa^2 u_D{}^2\,\mathrm{Ri} + m^2 + u_{Dy}\,\mathrm{Ri}) + m\frac{D_z}{D} \\
D &= -\kappa^2\,\mathrm{Ri}u_D{}^2 - m^2 + \mathrm{Ri} - u_{Dy}\,\mathrm{Ri}
\end{aligned}\right\} \quad \text{(A2)}$$

* In the classical Eady problem (quasi-geostrophic), only the underlined terms are present.

The transformation to η-coordinates implies the following substitutions in (A1):

$$b_{22} \rightarrow \frac{1}{(1-h)^2}[b_{22} + b_{12}h_y(\eta - 1) + b_{11}(\eta - 1)^2 h_y^2]$$

$$b_{12} \rightarrow \frac{1}{1-h}[b_{12} + 2b_{11}h_y(\eta - 1)]$$

$$b_2 \rightarrow \frac{1}{1-h}\left[b_2 + \frac{b_{12}h_y}{1-h} + (\eta - 1)\left(b_1 h_y + 2h_y^2 \frac{b_{11}}{1-h} + b_{11}h_{yy}\right)\right]$$

Finally,

$$C_1 = \frac{b_{11}}{b_{22}}, \quad C_2 = \frac{b_{12}}{b_{22}}, \quad C_3 = \frac{b_1}{b_{22}}, \quad C_4 = \frac{b_2}{b_{22}}, \quad C_5 = \frac{b}{b_{22}}$$

At $z = h$ ($u_D = mh - \underline{c}$):

$$\left.\begin{aligned} D_0 &= \frac{1}{\underline{1}-h}[\kappa^2 u_D^2 - \underline{1} + m_y h + m h_y - \mathrm{Ri} h_y^2 + h_y] \\ \alpha_0 &= (\mathrm{Ri} h_y - m)/D_0 \\ \beta_0 &= \frac{1}{\underline{u_D}}(m - \mathrm{Ri} h_y)/D_0 \end{aligned}\right\} \quad \text{(A3)}$$

At $z = 1$ ($u_D = \underline{m - c}$)

$$\left.\begin{aligned} D_1 &= \frac{1}{\underline{1}-h}[\kappa^2 u_D^2 - \underline{1} + m_y] \\ \alpha_1 &= -m/D_1 \\ \beta_1 &= \underline{m/(u_D D_1)} \end{aligned}\right\} \quad \text{(A4)}$$

REFERENCES

Bender, C. M., and S. A. Orszag, 1978: *Advanced Mathematical Methods for Scientists and Engineers.* McGraw-Hill, 593 pp.

Buzzi, A., and A. Speranza, 1986: A theory of deep cyclogenesis in the lee of the Alps. Part II: effect of finite topographic slope and height. *J. Atmos. Sci.*, **43,** 2826–2837.

Mesinger, F., and R. T. Pierrehumbert, 1985: Alpine lee cyclogenesis: numerical simulation and theory. *Scientific Conference on the Results of the Alpine Experiment (ALPEX)* Venice, WMO, October 1985.

Pierrehumbert, R. T., 1984: Linear results on the barrier effects of mesoscale mountains, *J. Atmos. Sci.*, **41,** 1356–1367.

——, and B. Wyman, 1985: Upstream effects of mesoscale mountains. *J. Atmos. Sci.*, **42,** 977–1003.

——, 1985: A theoretical model of orographically modified cyclogenesis. *J. Atmos. Sci.*, **42,** 1244–1258.

Radinovich, D., 1965: On forecasting of cyclogenesis in the West Mediterranean and other areas bounded by mountain ranges by baroclinic model. *Arch. Meteor. Geophys. Bioklim.*, **A14,** 279–299.

Simmons, A. J., 1974: The meridional scale of baroclinic waves. *J. Atmos. Sci.*, **31,** 1515–1525.

Smith, R. T., 1984: A theory of lee cyclogenesis. *J. Atmos. Sci.*, **41,** 1159–1168.

Speranza, A., M. Fantini and A. Buzzi, 1985a: The action of high and steep mountains on quasi-geostrophic baroclinic instability and Alpine cyclogenesis. *Arch. Meteor. Geophys. Bioklim. Ser. A,* **33,** 245–261.

——, A. Buzzi, A. Trevisan and P. Malguzzi, 1985b: A theory of deep cyclogenesis in the lee of the Alps: modifications of baroclinic instability by localized topography. Part I. *J. Atmos. Sci.*, **42,** 1521–1535.

Stone, H. P., 1966: On nongeostrophic baroclinic instability. *J. Atmos. Sci.*, **23,** 390–400.

——, 1969: The meridional structure of baroclinic waves. *J. Atmos. Sci.*, **26,** 376–389.

Tosi, E., M. Fantini and A. Trevisan, 1983: Numerical experiments on orographic cyclogenesis: relationship between the development of the lee cyclone and the basic flow characteristics. *Mon. Wea. Rev.*, **111,** 799–814.

Tibaldi, S., A. Buzzi and P. Malguzzi, 1980: Orographically induced cyclogenesis: analysis of numerical experiments. *Mon. Wea. Rev.*, **108,** 1302–1314.

Trevisan, A., M. Fantini and E. Tosi, 1984: Modeling Alpine Cyclogenesis in a two layer quasi-geostrophic model. *Riv. Meteorol. Aeronaut.*, **44,** 211–218.